

Supporting information for:

Endogenous Osteocyte-Osteoclast Signaling Enables Bone Remodeling, Drug Response, and Cancer Invasion in a Nanoscale Calcified Bone-on-a-Chip Model

Mauricio G.C. Sousa^{1,2,6} #, Avathamsa Athirasala^{1,2,6} #, Daniela M. Roth^{1,2,6}, Mahshid Hosseini^{1,2,6}, Genevieve E. Romanowicz⁹ Rebekka Duhem^{1,2} May Anny A. Fraga⁷, Sofia M. Vignolo^{1,3,5}, Aaron Doe², Jinho Lee⁸, Jonathan V. Nguyen⁶, Angela S.P. Lin⁷, Cristiane M. Franca^{1,6}, Robert E. Guldberg⁹, Luiz E. Bertassoni^{1,3,4,5,6}

¹ Knight Cancer Precision Biofabrication Hub, Cancer Early Detection Advanced Research (CEDAR), Knight Cancer Institute, Oregon Health & Science University, Portland, Oregon, USA.

² Division of Oncological Sciences, Knight Cancer Institute, Oregon Health & Science University, Portland, Oregon, USA.

³ Center for Regenerative Medicine, School of Medicine, Oregon Health & Science University, Portland, Oregon, USA.

⁴ Department of Biomedical Engineering, School of Medicine, Oregon Health & Science University, Portland, Oregon, USA.

⁵ Department of Oral Rehabilitation and Biosciences, School of Dentistry, Oregon Health & Science University, Portland, Oregon, USA.

⁶ Department of Restorative Dentistry, Faculdade de Odontologia de Piracicaba (FOP), Universidade Estadual de Campinas, Piracicaba, São Paulo, Brazil.

⁷ Knight Campus for Accelerating Scientific Impact, University of Oregon, Eugene, Oregon, USA.

Corresponding author:

Luiz E. Bertassoni

Email: bertasso@ohsu.edu

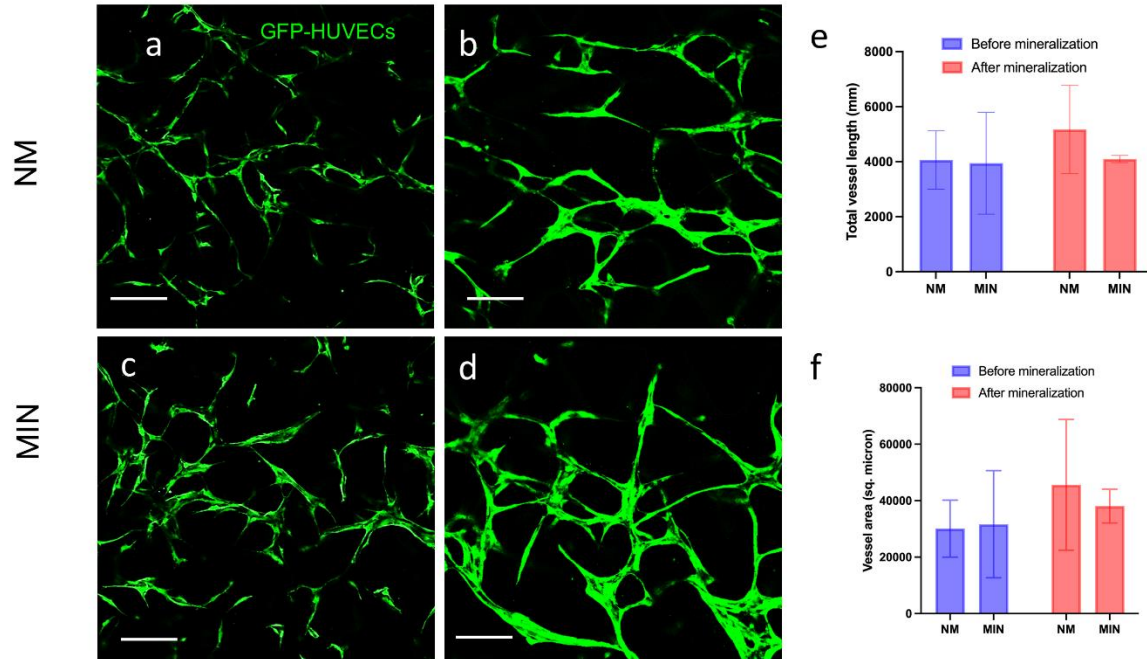


Figure S1. Bone-on-a-chip supports the addition of functional vessels without the influence of mineralization. Representative images (a-d) showing comparable endothelial capillary network formation by GFP-expressing HUVECs (Angioproteomie) encapsulated in non-mineralized (a-b) and mineralized samples (c-d) on day 2 (a, c-30 μm) and day 5 (b, d-10 μm) of culture. Quantification of the total vessel length (e) and vessel area (f) showed no significant differences among mineralized and non-mineralized samples before or after mineralization.

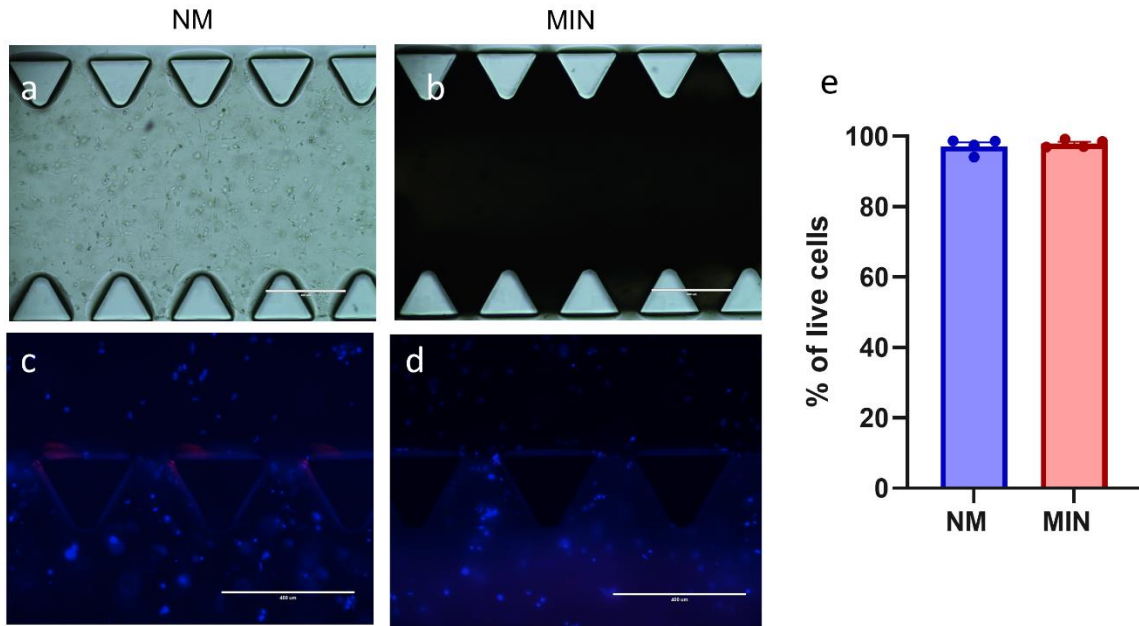


Figure S2. Characterization of on chip mineralization process and associated cellular viability. Incorporation of calcium phosphate in the mineralized groups is evident from the change in opacity in phase contrast images (a,b) when compared to the non-mineralized samples. Representative images (a,b) of chips treated with Hoechst (live, blue) and propidium iodide (dead, red) following 5 days of culture in non-mineralized (NM) and mineralized (MIN) conditions showed minimal cell death in both groups, with (c) no statistically significant difference in viability between the groups after a t-test analysis (N=4). Scale bars in a-d represent 400 μm .

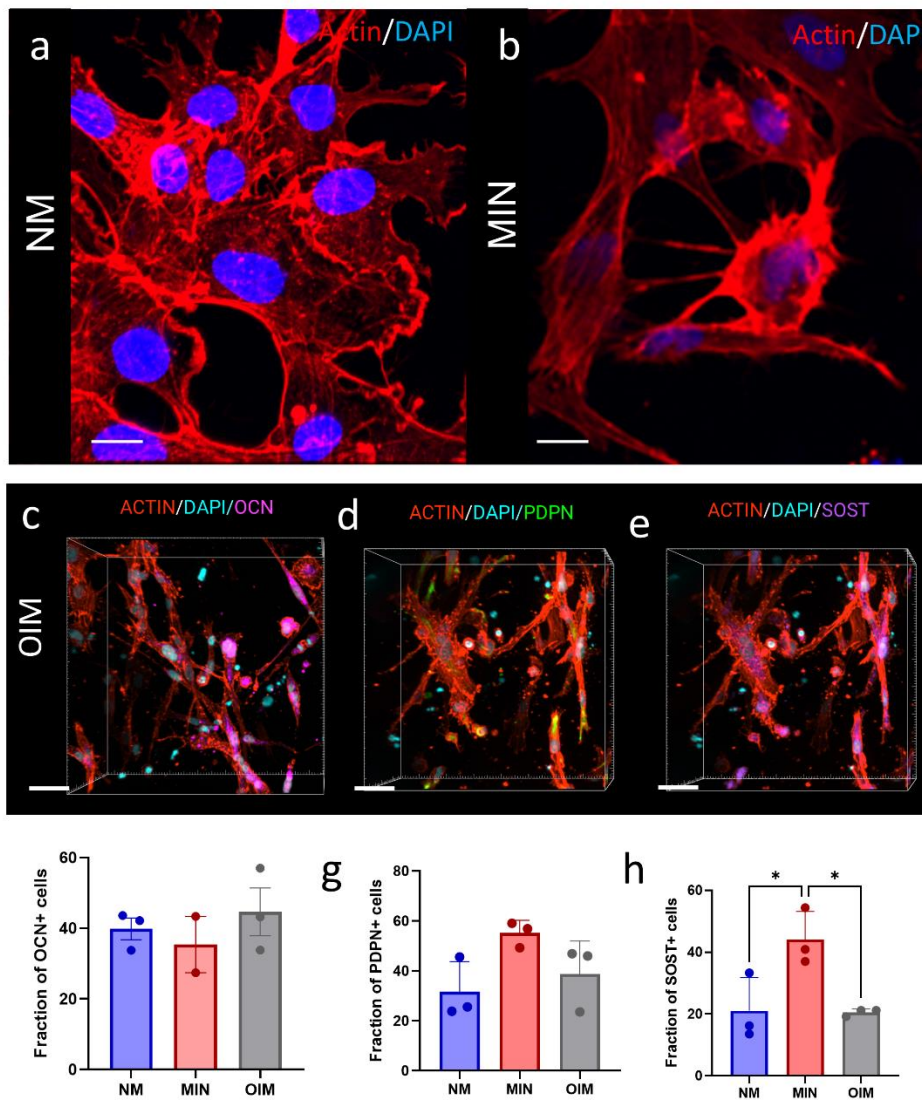


Figure S3. Bone-on-a-chip promotes rapid osteoblast-to-osteocyte differentiation. Representative confocal images (a,b) of samples stained for F-actin (red) and DAPI (blue) after 3 days in culture show distinct cellular morphologies between mineralized and non-mineralized conditions, with mineralized samples displaying cell dentrite-like structures consistent with osteocyte network formation. Expression of osteocyte-associated markers OCN (magenta; c), PDPN (green; d), and SOST (magenta; e) was assessed after 7 days in osteoinductive medium (OIM). Quantification (f–h) shows significantly higher SOST expression in mineralized samples compared with OIM and non-mineralized groups. Statistical significance was determined by one-way ANOVA with Tukey’s correction (* $p < 0.05$). Scale bars, 10 μm (a,b) and 20 μm (c–e).

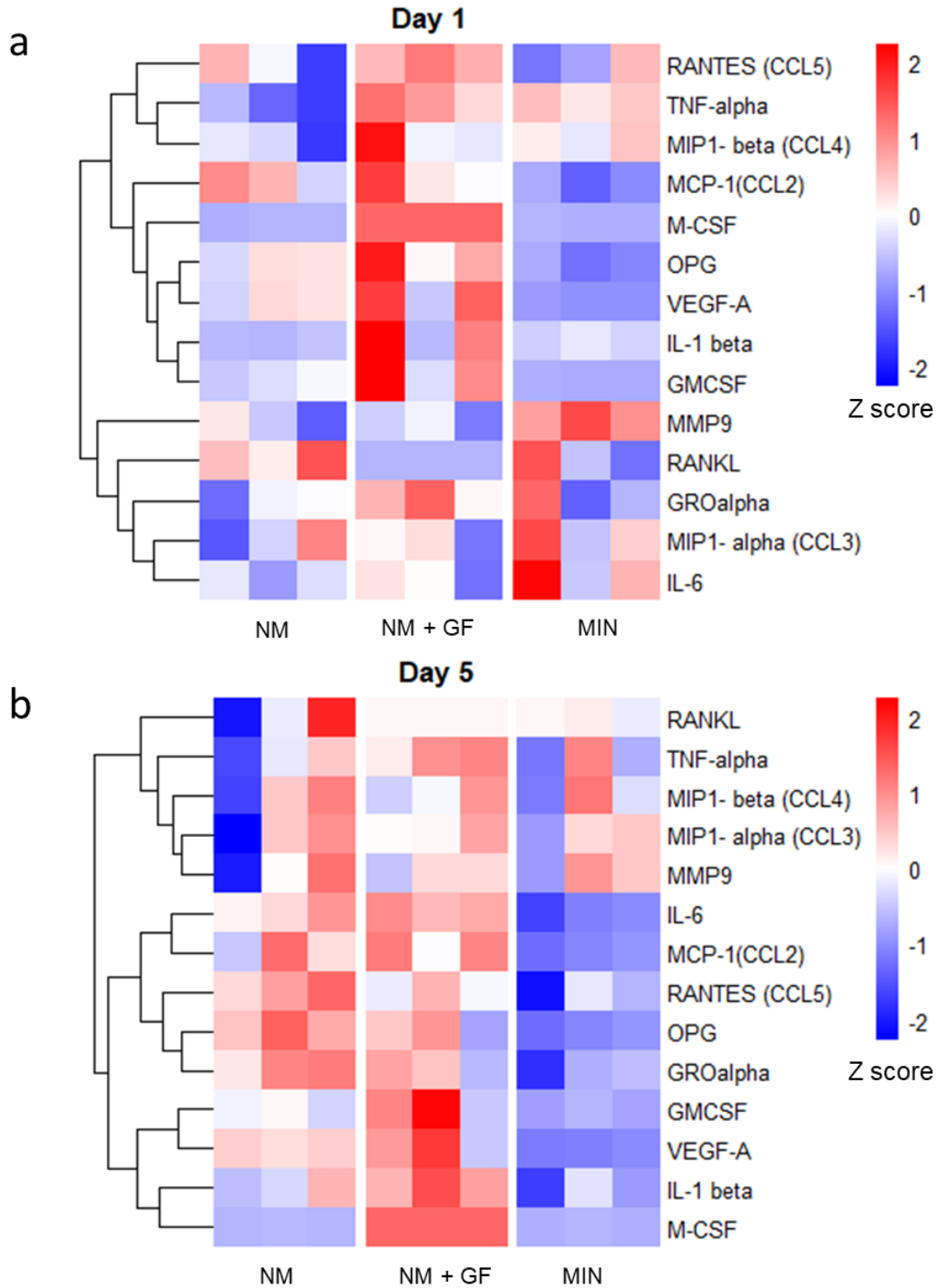


Figure S4. Relative secretion profiles of osteoclastogenic cytokines in mineralized and non-mineralized bone-on-a-chip cultures. Heatmaps showing relative secretion of 13 proteins/cytokines and chemokines in the supernatants of non-mineralized (NM), non-mineralized + RANKL/M-CSF (NM + GF), and mineralized (MIN) samples after 1 (a) or 5 days (b) of culture as measured by Luminex multiplex analysis. The results are presented as Z-scores, with measurements obtained from 3 different biological replicates.

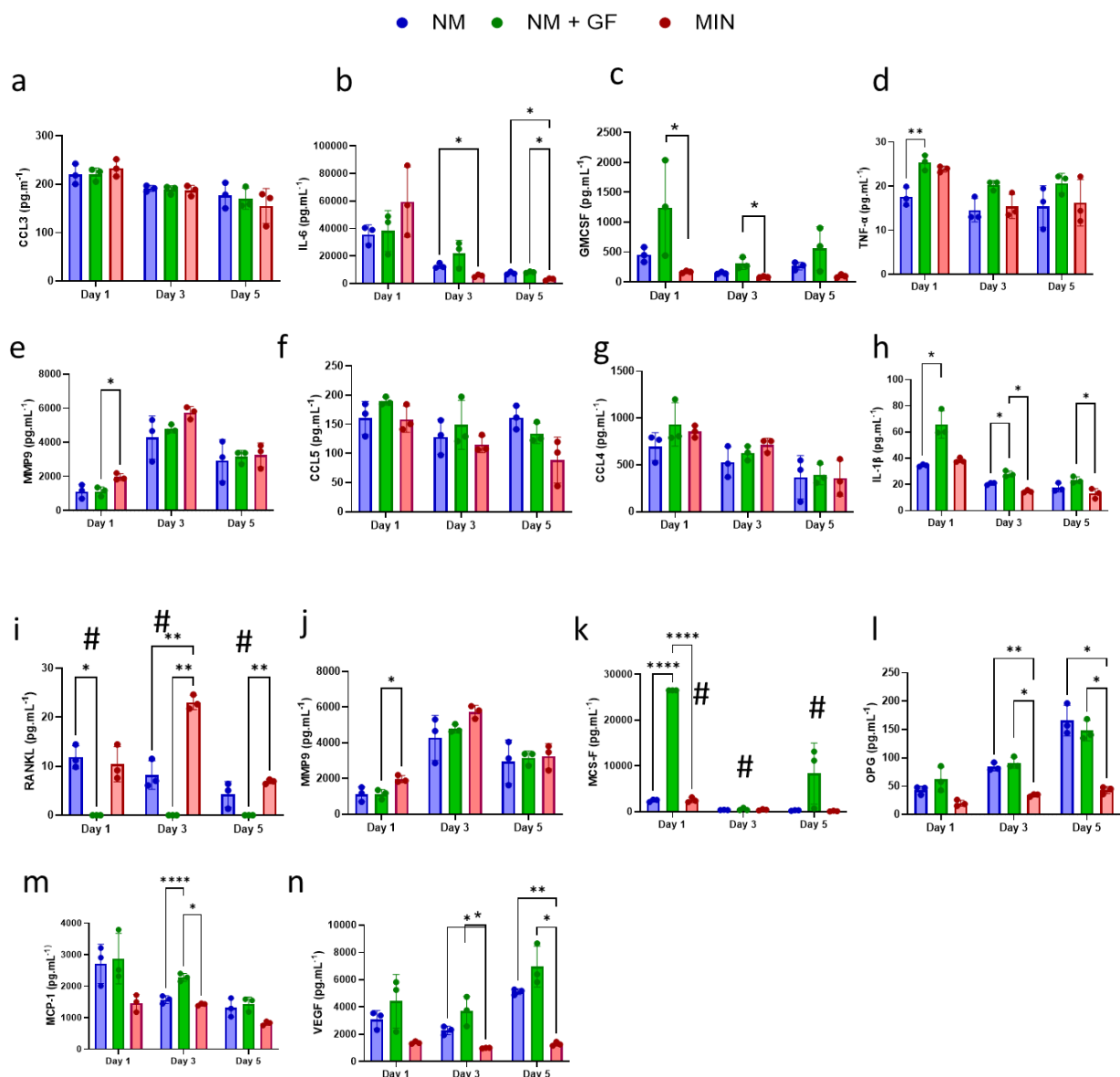


Figure S5. Proteins/cytokines and chemokines related to osteoclastogenesis in solution after 1, 3, or 5 days of culture as measured by Luminex multiplex analysis. The average total production of proteins/cytokines (N=3) is represented in pg.mL⁻¹. Significant statistical differences are represented by * p<0.05, ** p<0.01, *** p<0.001, and **** p<0.0001 after one-way ANOVA with Tukey's correction. # represents groups that already had RANKL (50 ng.mL⁻¹) and M-CSF (30 ng.mL⁻¹) in the media. These known concentrations in the media were subtracted from the measured Luminex values.

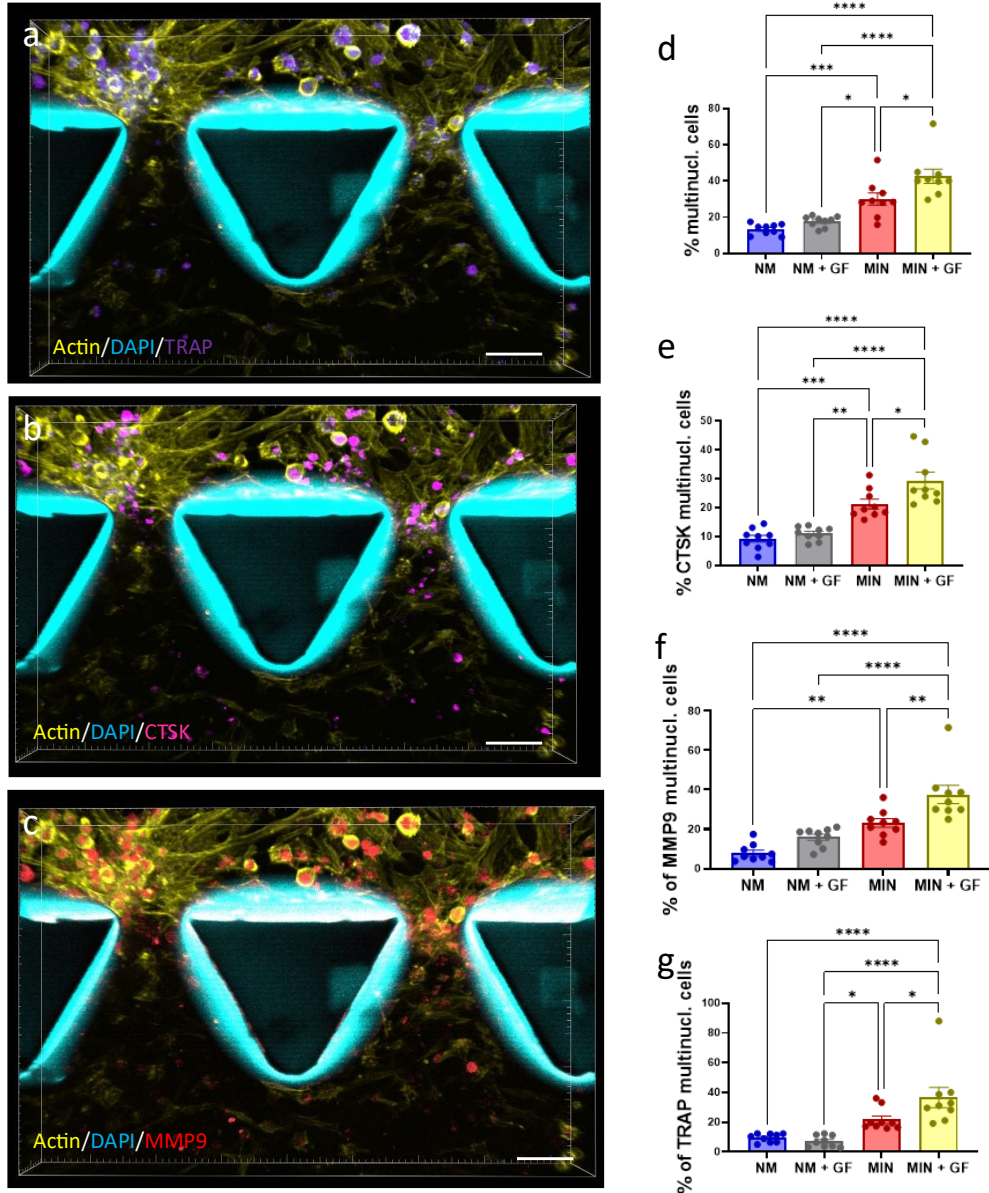


Figure S6. Osteoclast differentiation in the bone-on-a-chip is enhanced by mineralization and supplemented RANKL/M-CSF. Representative confocal images (a-c) of mineralized samples treated with RANKL (50 ng/ml) and M-CSF (30 ng/ml) supplemented media, show cells positive for TRAP, CTSK, and MMP9. Graphs (d-g) illustrate the increase in osteoclast numbers depending on mineralization and the addition of growth factors (GF). Mineralized samples supplemented with GF exhibited the highest number of multinucleated cells and TRAP-, CTSK-, and MMP9-positive osteoclasts, indicating that RANKL and M-CSF further promote osteoclastogenesis of macrophage-derived progenitors under mineralized conditions. Statistical significance in (e-g) is indicated as * $p < 0.05$, ** $p < 0.01$, *** $p < 0.001$, **** $p < 0.0001$ (one-way ANOVA with Tukey's correction).

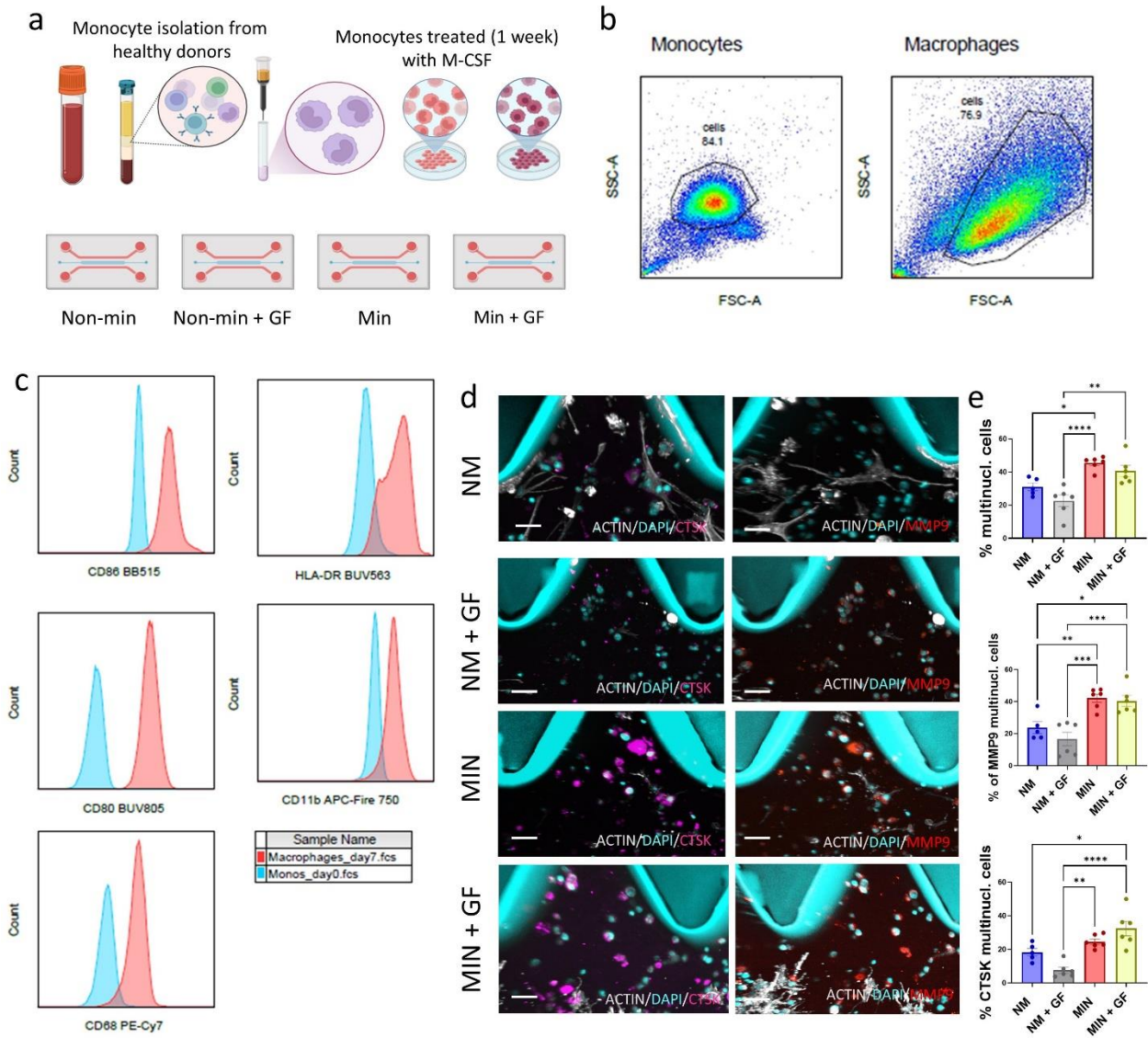


Figure S7. Osteoclastogenesis on-a-chip using primary human cells. Primary human monocytes were isolated from healthy donors (a) and differentiated into macrophages with M-CSF for 7 days off-chip. Flow cytometry dot plots (b) show changes in cell size and granularity following differentiation, while histograms (c) confirm distinct surface marker expression between monocytes and macrophages (CD86, HLA-DR, CD80, CD11b, CD68). Differentiated macrophages were seeded into the lateral channel of the chip and cultured for 5 days, followed by fixation and staining for cathepsin K (CTSK) and matrix metalloproteinase-9 (MMP9). Representative images (d) show increased CTSK- and MMP9-positive cells under mineralized (MIN) and mineralized plus growth factors (MIN + GF) conditions. Quantification (e) shows higher proportions of multinucleated cells and CTSK and MMP9 positivity in MIN and MIN + GF groups. Scale bar, 20 μm . Statistical analysis was performed using one-way ANOVA with Tukey's correction (* $p < 0.05$, ** $p < 0.01$, *** $p < 0.001$, **** $p < 0.0001$).

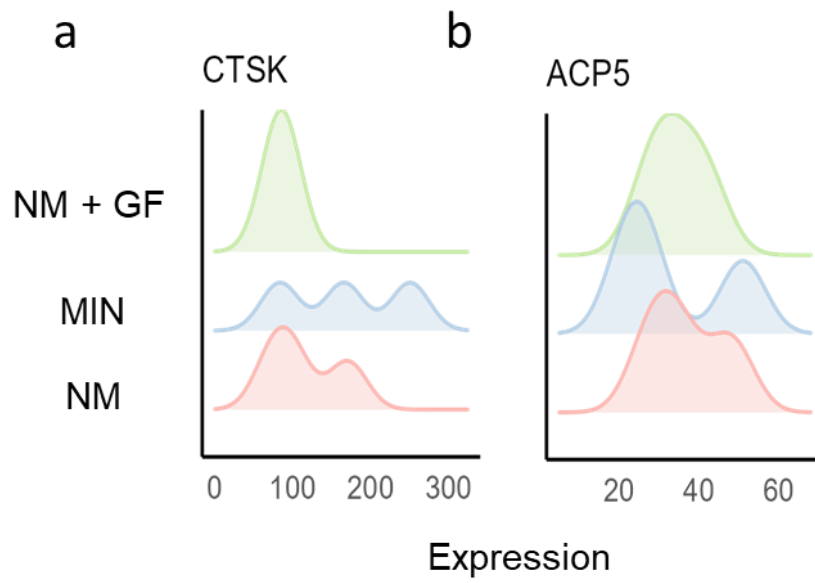


Figure S8. Ridge plot showing the known osteoclast marker genes CTSK and ACP5. NM: non-mineralized; MIN: mineralized; and NM + GF: non-mineralized with RANKL and M-CSF.

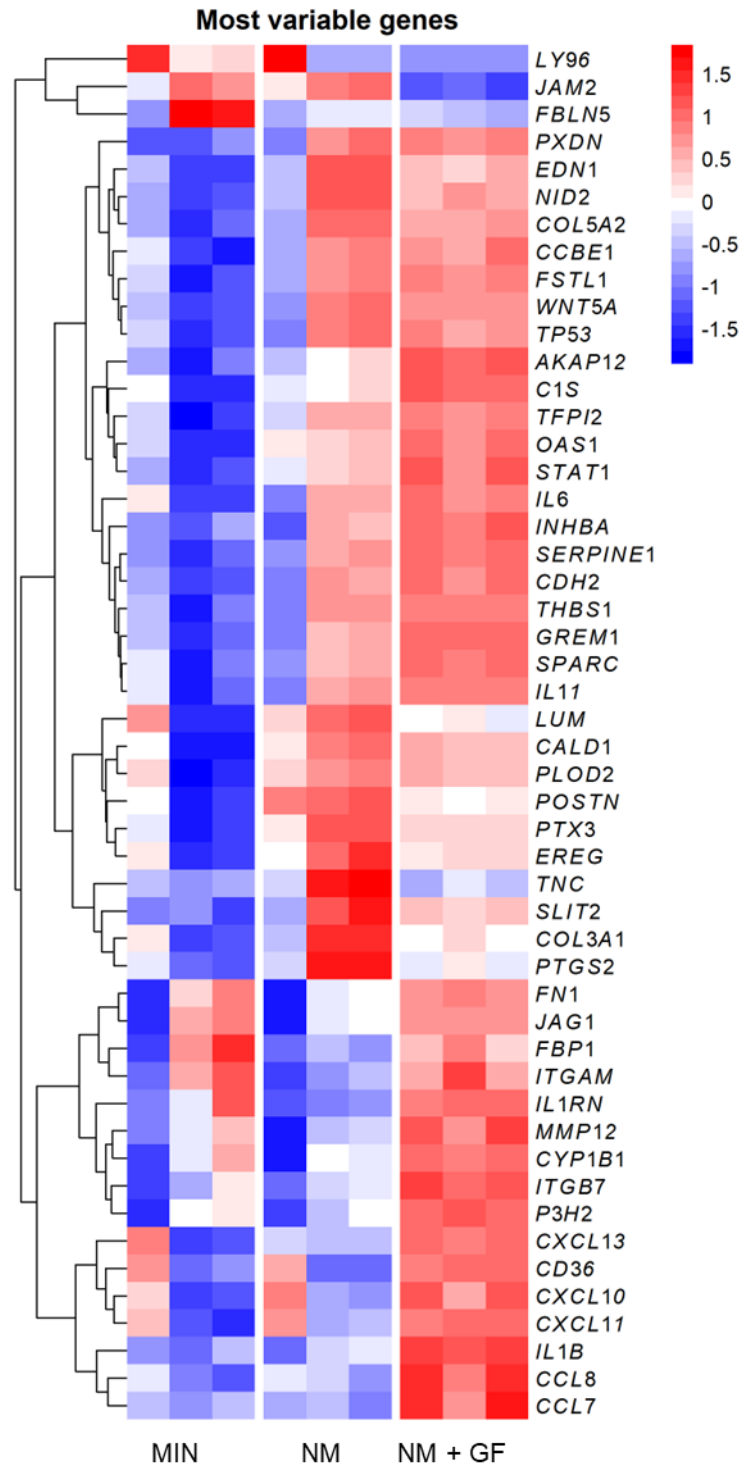


Figure S9. Heatmap of the top 50 differentially expressed genes for the mineralized (MIN), non-mineralized (NM), and non-mineralized with RANKL/M-CSF (NM + GF). Color intensity represents the log₂ (fold change), with red indicating higher expression and blue indicating low expression across 3 biological replicates.

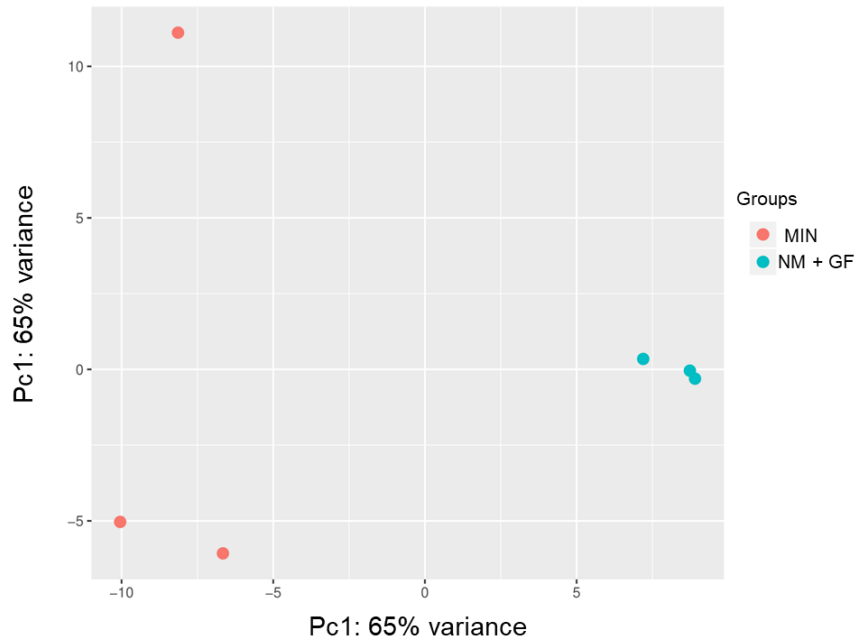


Figure S10. Principal component analysis comparing the group with RANKL/M-CSF (NM + GF, green dots) with the mineralized group (MIN, orange dots). Each dot represents a different replicate, and the data shows a clear separation between the 2 groups, clustering mainly in the different replicates of the RANKL + M-CSF groups.

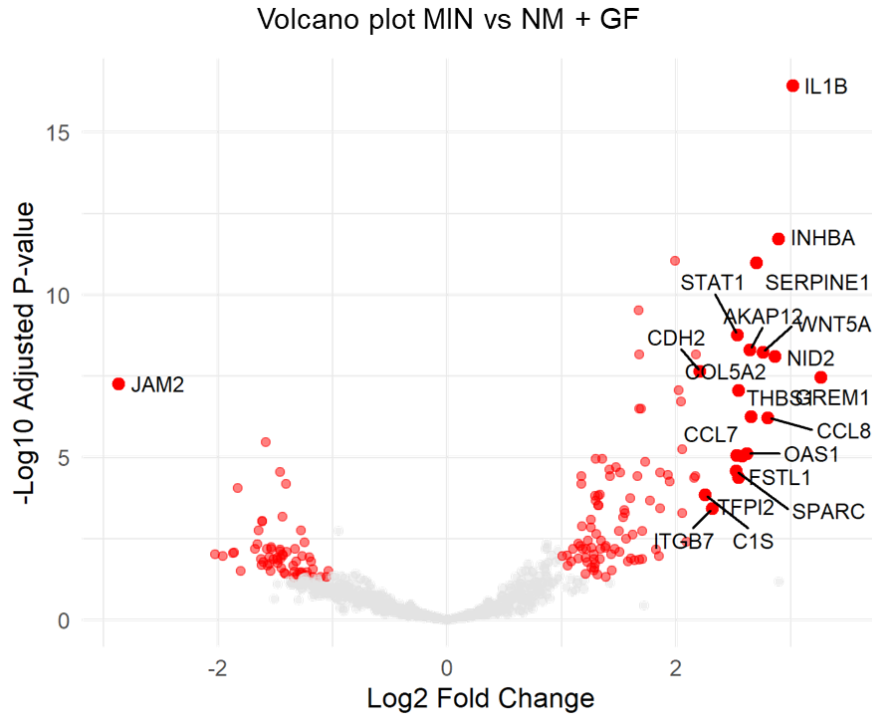


Figure S11. Volcano Plot shows the comparison of gene expressions in log₂ fold change among the 770 genes from the pan-cancer progression panel (ncounter nanostring), between the mineralized (MIN, left red dots) and non-mineralized with RANKL/M-CSF (NM + GF, right red dots). The results show the expression of inflammation-related genes in RANK groups, such as IL-1 β , and genes related to cellular adhesion/matrix, such as JAM2, for mineralized groups.

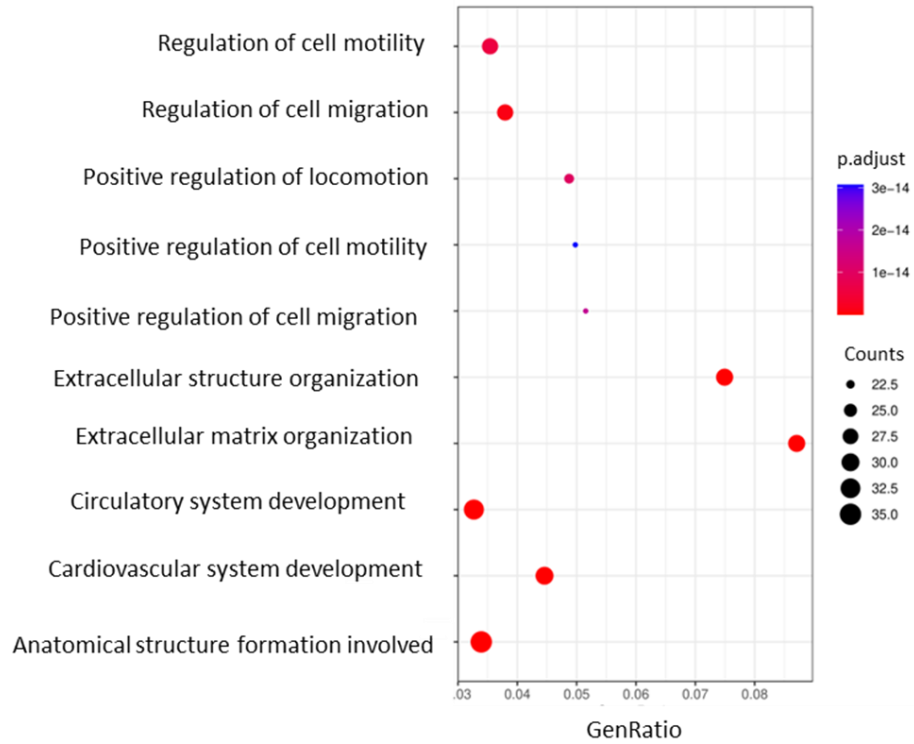


Figure S12. Gene ontology (GO) enrichment analysis using different expressed genes in mineralized groups (MIN) compared to the RANKL/M-CSF groups (NM + GF). The y-axis represents gene functions, with dots indicating the gene ratio (x-axis) based on the number of counts. The color gradient, ranging from red to blue, represents the p.adjust variation.

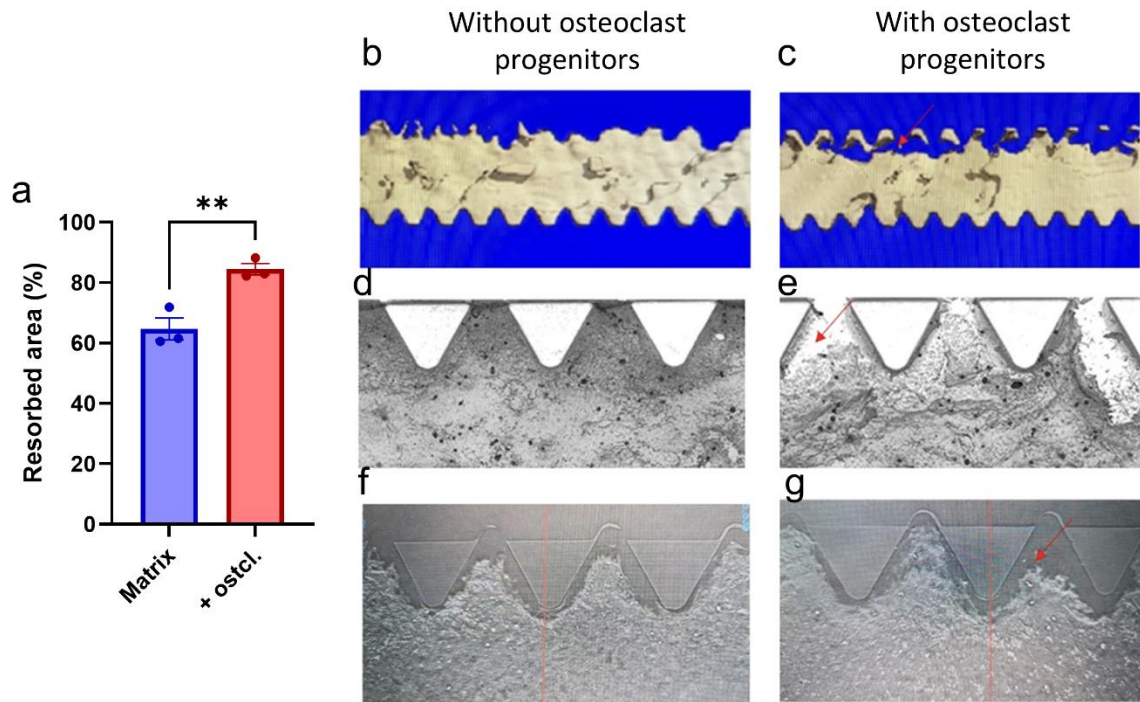


Figure S13. Bone-on-a-chip-generated osteoclasts exhibit functional matrix resorption. Mineralized matrix remodeling in the presence or absence of osteoclast progenitors is shown in the second harmonic generation microscope (a). Representative 3D micro-CT reconstructions and transmission images of mineralized chips cultured without (b, d, f) or with osteoclast progenitors (c, e, g) reveal distinct resorption pits in progenitor-containing conditions (red arrows).

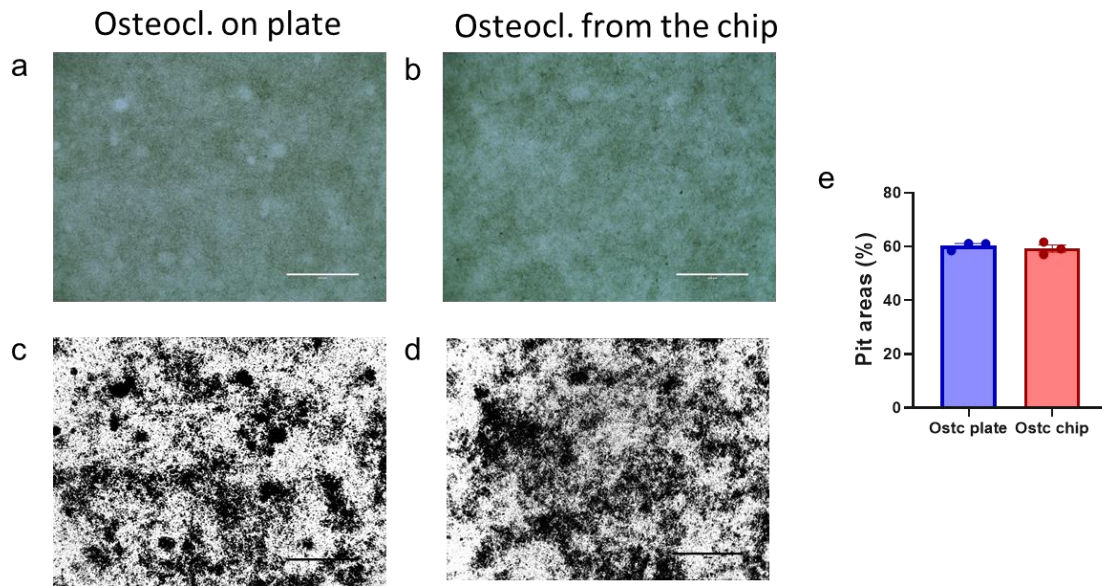


Figure S14. Chip-derived osteoclasts are functional on CaP plates. Functional activity of osteoclasts differentiated on mineralized matrices in chips before being retrieved and seeded on CaP plates for 3 days (a,c) was compared to that of osteoclasts derived from macrophages cultured on CaP plates for 14 days in media supplemented with RANKL (50 ng/mL) and M-CSF (30 ng/mL) for 14 days (b,d). Resorbed pit area fraction (e) quantified from a bright field image converted to high contrast binary images in ImageJ according to AMSBIO (Life Science and Product Solutions) guidelines showed no significant differences between osteoclasts differentiated directly on the plate or osteoclasts from the chip.

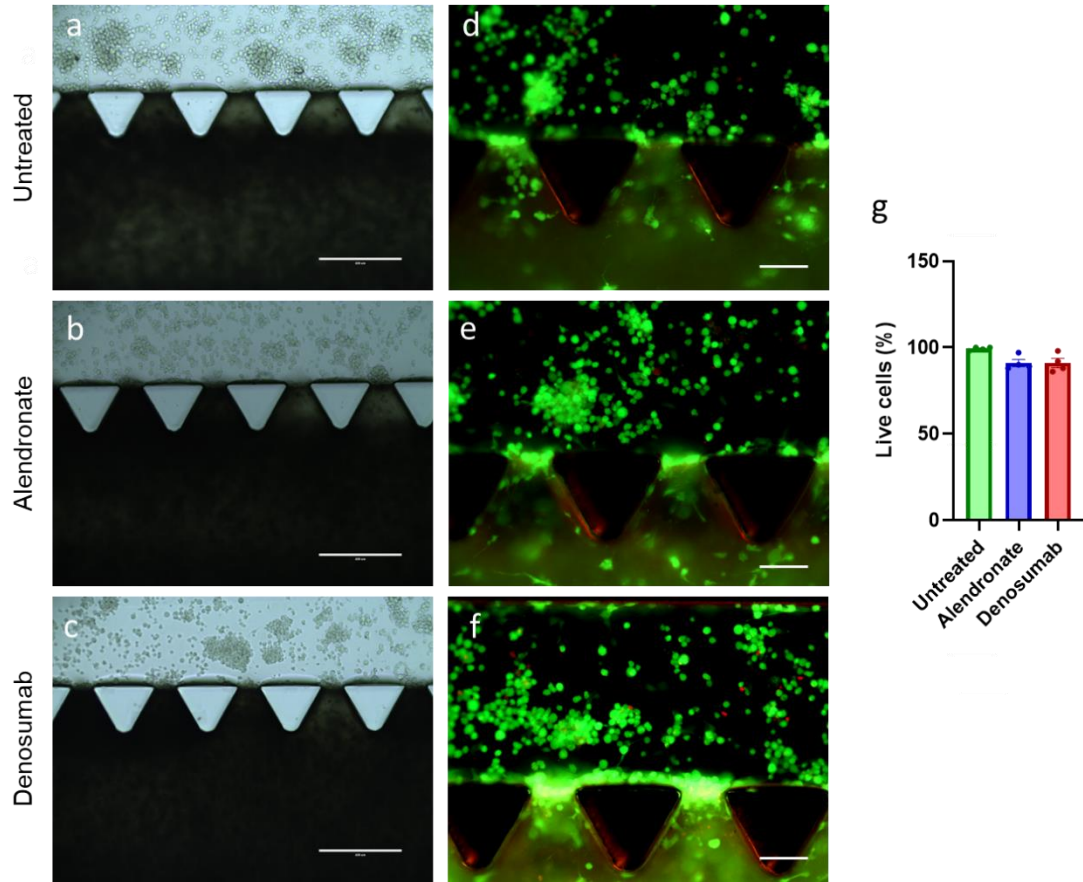


Figure S15. Cellular viability after drug treatment. Representative phase contrast images (a-c) of mineralized chips where macrophages received no treatment (a), alendronate (b), or denosumab (c) showed comparable cell numbers. Cell viability assessed by calcein AM (live, green) and propidium iodide (dead, red) staining (d-f) showed (g) no significant differences in cell viability between the groups (N = 3) after 5 days of treatment. Scale bars represent 400 μ m.

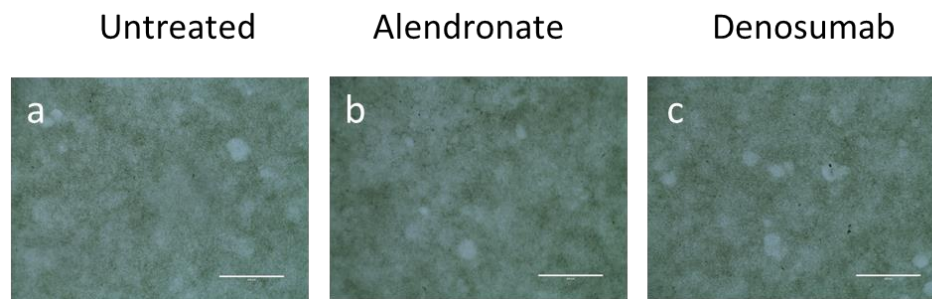


Figure S16. Functional assessment of osteoclasts differentiated on CaP plates following drug treatment. Pit areas on CaP-coated plates after seeding macrophages (with 50 ng.mL^{-1} of RANKL and 30 ng.mL^{-1}) and treating the samples for 14 days with alendronate or denosumab. c-d shows the phase-contrast image of the samples (N=3). Scale bars represent $400 \text{ }\mu\text{m}$.

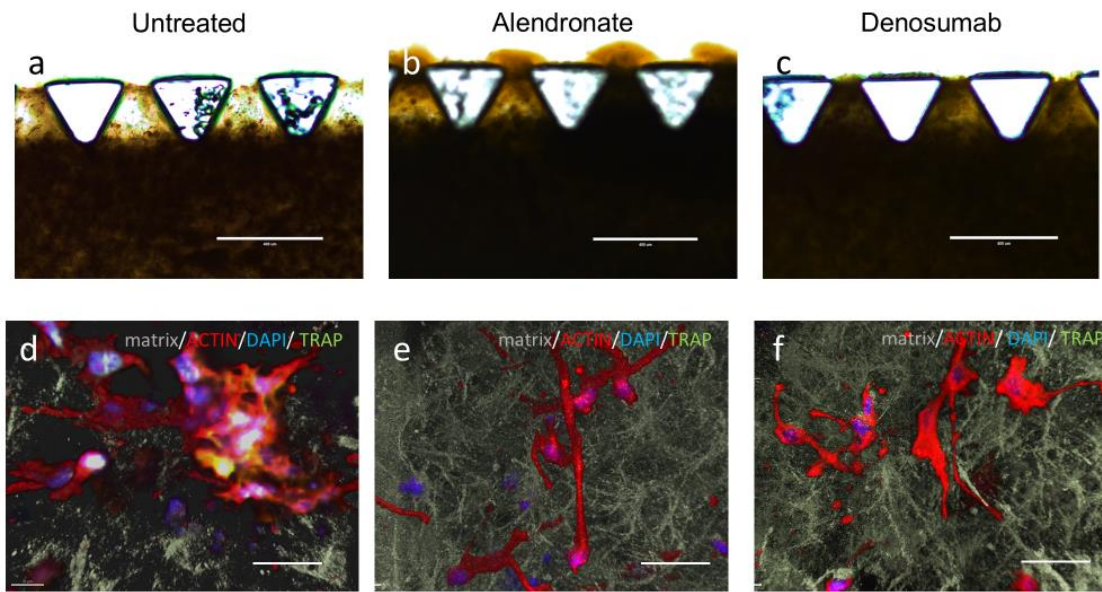


Figure S17. Alizarin red and confocal image screening of bone resorption on bone-on-a-chip treated with anti-resorption drugs. Alizarin red staining of bone-mimetic environments shows higher resorption of mineralized matrix in untreated samples (a) when compared to samples treated with alendronate (b) or denosumab (c), demonstrating the ability of the model to capture drug-specific effects on bone resorption in vitro. Scale bars: 400 μm . Panels (d–f) show cell–matrix interactions with actin, DAPI, and TRAP staining in untreated (d), alendronate-treated (e), and denosumab-treated (f) samples, revealing reduced TRAP expression in both drug-treated groups.

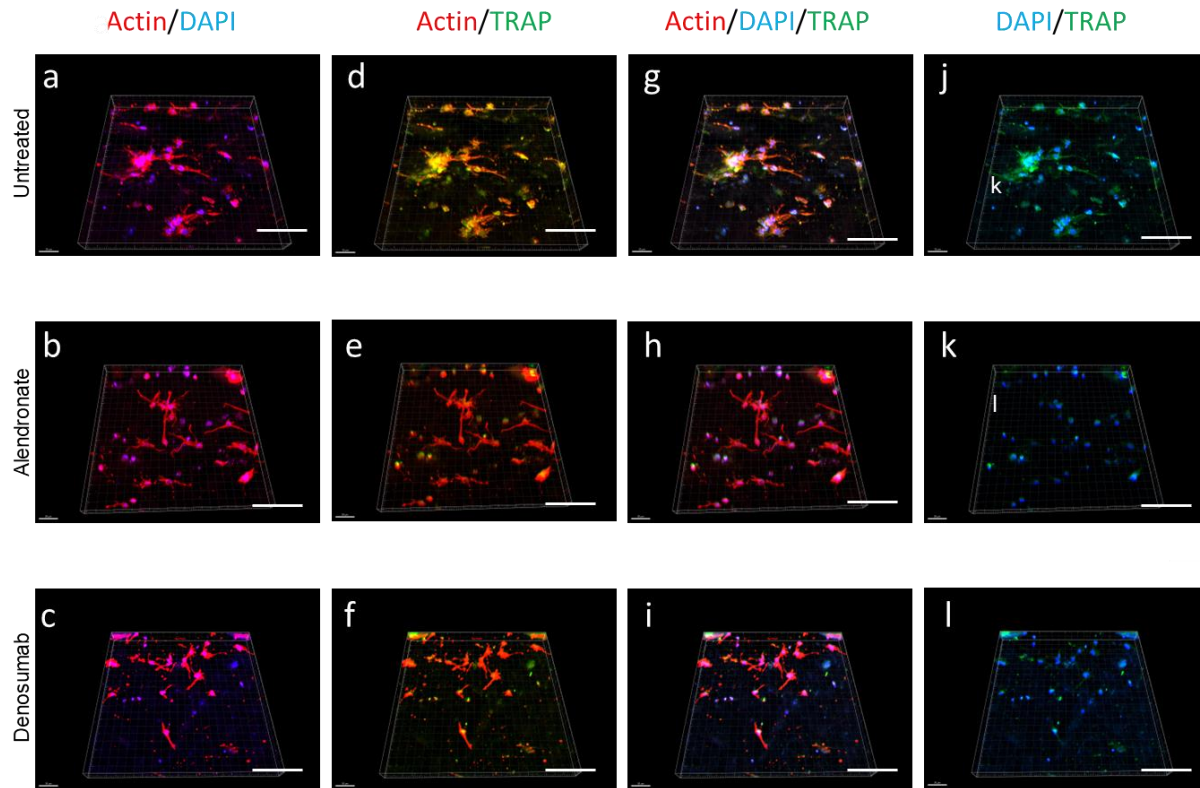


Figure S18. Bone-on-a-chip models osteoclast-targeting drug responses through reduced TRAP expression. Representative lower magnification images of mineralized chips treated with alendronate (b, e, h, k) or denosumab (c, f, i, l) for 5 days (N=3) and immunostained for actin, DAPI, and TRAP. Reduced TRAP expression in drug-treated groups, alendronate (b-k) and denosumab (c-l), highlighting the platform's capacity to model osteoclast-targeting drug responses. The scale bars represent 150 μm .

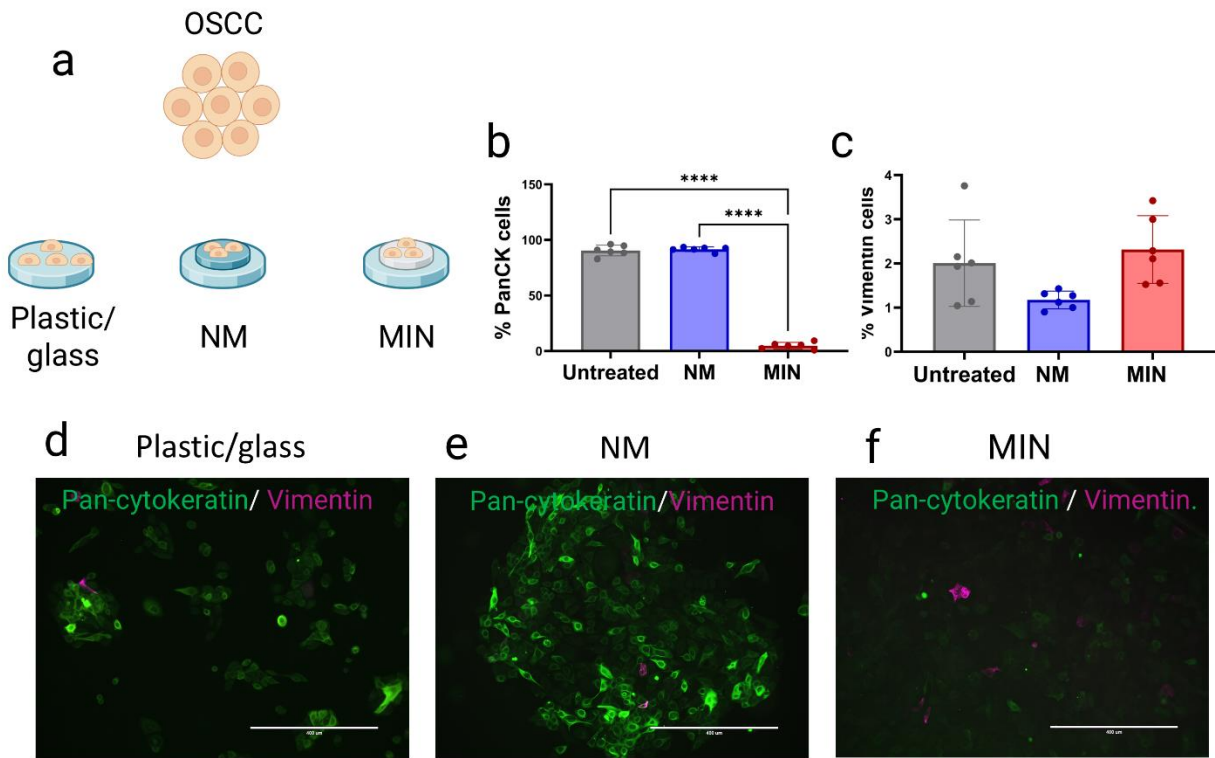


Figure S19. Mineralized matrix promotes loss of Pan-cytokeratin in OSCC cells off chip. UCSF-OT-1109 OSCC cells were seeded onto collagen disks that were either mineralized or non-mineralized, as well as on tissue culture plastic. After 3 days, samples were fixed and immunostained for pan-cytokeratin (PanCK, green) and vimentin (magenta) (a). Quantification (b) reveals a significant reduction in PanCK expression in cells on mineralized collagen (f) compared with non-mineralized collagen (e) or plastic (d). Scale bars in (d–f) represent 400 μm . Statistical significance was determined by one-way ANOVA with Tukey’s post hoc test (**** $p < 0.0001$).

Supporting Video 1. Mineralized bone-on-a-chip supports vascular and osteoclast compartments.

Representative 3D visualization showing a mineralized bone-on-a-chip incorporating vascular and osteoclast components. Vascular networks were formed by co-culturing mesenchymal stem cells and human umbilical vein endothelial cells (HUVECs), together with osteoblasts. After 3 days of mineralization, the system exhibits lumenized vessel structures and osteocyte differentiation. Macrophages were introduced into the lateral channel and differentiated into osteoclasts. Vessels are labeled by CD31 (orange), osteocytes by PDPN (yellow), osteoclasts by cathepsin K (CTSK; purple), and nuclei by DAPI (blue).

Supporting Video 2. Pre-osteoclast fusion within a mineralized osteocyte environment. The video captures the early stages of macrophage fusion on mineralized substrates after 6 hours of incubation in an osteocyte-laden mineralized matrix. Cells were fluorescently labeled with DAPI (nuclei, blue), actin (cytoskeleton, red), and the osteoclast-specific marker TRAP antibody (green), enabling visualization of multinucleated pre-osteoclast formation within a physiologically relevant microenvironment.

Supporting Video 3. Remodeling niches in osteocyte–osteoclast co-cultures. This video demonstrates the dynamic remodeling regions formed within mineralized bone-like matrices following 5 days of macrophage seeding in the lateral channel. Osteoclasts (TRAP-positive, green; actin-positive, red; DAPI-positive, blue) are observed interacting directly with osteocytes (actin-positive, red; DAPI-positive, blue) embedded within the mineralized matrix (grey), imaged by second harmonic generation microscopy. These localized remodeling zones highlights the power of this platform to recapitulate osteocyte–matrix–osteoclast interactions and provide unique insights into bone remodeling processes.